Ain Shams Engineering Journal 11 (2020) 751–765

Contents lists available at ScienceDirect

Ain Shams Engineering Journal

journal homepage: www.sciencedirect.com

Civil Engineering

Performance of reinforced self-consolidating concrete beam-column joints with headed bars subjected to pseudo-static cyclic loading

Abdul Hossein Paknejadi [a,*], Kiachehr Behfarnia [b]

[a] Pardis College, Civil Engineering Group, Isfahan University of Technology, Isfahan 84156-83111, Iran
[b] Department of Civil Engineering, Isfahan University of Technology, Isfahan 84156-83111, Iran

ARTICLE INFO

Article history:
Received 27 April 2019
Revised 12 December 2019
Accepted 31 December 2019
Available online 28 January 2020

Keywords:
Headed bar
Self-consolidating concrete
Exterior beam-column joint
Cyclic loading
Seismic criteria
Relative head area

ABSTRACT

With the growing use of headed bars in the RC beam-column joints to reduce reinforcement congestion in the joint region, more tests are needed to gain further insight into the behavior of these joints and perfect the related design codes. Given the limitations imposed in ACI318-14 on the type of concrete and the relative head area, which is the net bearing area of the head divided by the bar area, this study investigated the effect of these parameters by testing four interstory exterior joint specimens constructed at the $\frac{2}{3}$scale under cyclic loading. These tests investigated the compliance of the joints with the seismic criteria when: (1) the joint was made with the self-consolidating concrete instead of the normal one, and (2) the joint was designed with the relative head area set to 3 instead of 4. The results showed that the use of the self-consolidating concrete improved the seismic behavior of the joint and reducing the relative head area to 3 did not render the joint performance unacceptable.

1. Introduction

Joints are among the major determinants of the performance of RC structures under cyclic loads. Seismic behavior of joints in building frames has been investigated by many researchers [1–3]. Given the congestion of reinforcements in and around the joints, especially the exterior ones, which can undermine the placement and consolidation of concrete, any solution for reducing the reinforcement congestion in the joint region could be of high practical value. There are some solutions to the congestion problem, with the most notable ones being the use of headed bars instead of hook bars and the replacement of the normal concrete (NC) with the self-consolidating concrete (SCC). The pullout and anchorage capacity of headed bars has been extensively studied at the universities of Calgary [4], Kansas [5], and Texas at Austin [6–8]. Research on factors such as anchorage length, clear spacing, rebar placement, geometry, head dimensions, and the details of the anchorage region has proved that the anchorage capacity strongly depends on the relative head area, or A_{brg}/A_b where A_{brg} is the net bearing area of the head and A_b is the bar area. Overall, these studies have found that the greater the relative head area, the higher the tensile stress capacity of the head. Pullout tests have also shown that the heads with A_{brg}/A_b of more than 2.6 can have a notable impact on load bearing, even after significant bond failure [9]. It has also been proved that regardless of the geometric shape and the attachment technique used, the heads provide acceptable anchorage and can fully transfer the design forces. In the experiments conducted in the early 1990s by Wallace et al. [10], beam-column joint specimens with headed bars were subjected to cyclic loading to investigate the application of these bars in the seismic areas. These experiments were performed on two specimens of exterior joints and three specimens of roof knee joints with tapered-threaded and friction-welded headed bars. The results suggested that the specimens with headed bars behaved at least as well as and sometimes better than hooks. Based on the experimental results, this research recommended an anchorage length of at least $12d_b$ and a relative head area of at least 4 for the studied joints [8]. In another study, Kang et al. [11] studied the beam-column joints with header bars, paying close attention to the spacing between beam bars. These researchers applied cyclic loading on two large-scale specimens of the exterior beam-column joint,

* Corresponding author at: Pardis College, Civil Engineering Group, Isfahan University of Technology, Isfahan 84156-83111, Iran.
E-mail address: a.paknejadi@pa.iut.ac.ir (A.H. Paknejadi).

Peer review under responsibility of Ain Shams University.

Production and hosting by Elsevier

https://doi.org/10.1016/j.asej.2019.12.008
2090-4479/

one with a single horizontal row of headed bars with the clear spacing of $2.11d_b$ and the other with two horizontal rows of headed bars at the top and bottom of the beam with the vertical spacing of $1.33d_b$. The results showed that both specimens largely met the seismic requirements specified in ACI 374.1-05 [12]. This study concluded that, for the exterior beam-column joints, using headed bars with the clear spacing of $2d_b$, where d_b is the bar diameter, or two layers of headed bars was permissible.

Tests were also conducted on tensile and flexural specimens having splices 25 mm in diameter and headed bars with $70 \times 70 \times 16$ mm friction welded heads. The net head bearing area was 9 times more than the bar diameter, which would be sufficient to develop the full bar yield strength by bearing, without any contribution from the bond along the bar [13,14].

Chien-Kuo Chiu et al. [15] studied the seismic anchorage behavior of headed bars using 12 groups of the full-size specimens of exterior and interior beam–column joints. They suggested design requirements for headed bars in such joints. Additionally, the application of headed bars with spliced and butted types on the interior beam–column joints was also studied in this work. Based on the obtained results, the minimal required net spacing of the headed bars could be set at $2.2d_b$.

Hung-Jen Lee et al. [16] investigated alternative reinforcing details for the bottom bars of precast concrete beams at the cast-in-place beam–column joints to achieve the behavior for monolithic reinforced concrete beam–column connections. To relieve steel congestion and fabrication difficulties, it was proposed to use headed bars for the bottom bars protruded from precast beams and anchored in the middle of the beam–column joint.

In another study, Jean Paul Vella et al. [17] suggested design recommendations and practical applications for headed bar connections between precast concrete elements. Design recommendations were made for narrow cast in–situ joints between the precast concrete slabs in which the continuity of reinforcement was achieved through overlapping headed bars.

Sung Chul Chun [18] used twenty-four beams reinforced with lap-spliced headed bars and tested them with 550 MPa headed bars, 62 MPa concrete strength, the small bar spacing of d_b, and transverse reinforcement. All specimens showed splitting failure with bottom cover spalling, which was in contradiction to the Section R12.6 of ACI318-11; transverse reinforcement was shown to be effective on improving the anchorage of the headed bars.

Lungui Li and Zhengxuan Jiang [19] studied five beam specimens with various headed bar details and a continuous reinforced specimen under flexure loadings were tested. A headed bar detail with 152 mm lap length was recommended.

In a series of tests by Yang [20], the use of commercially available headed deformed bars in beams with the depths of 460, 610, and 915 mm. was investigated. The results indicated that headed deformed bars could be used as the shear reinforcement, even when the net bearing area of the heads approached the ACI 318-14 lower limit of $4A_b$. Their specimens had concrete compressive strengths near 35 MPa and heads engaging the longitudinal reinforcement.

Lequesne, R et al. [21] tested thirty-nine beams with a shear span-to-depth ratio of 3 to determine whether headed deformed bars could be used in the reinforced concrete members in place of the stirrups as the shear reinforcement and whether shear reinforcement with yield strengths up to 550 MPa could be used without the problems related to the strength or serviceability. The results showed that the members with adequately anchored headed deformed bars had shear strengths equivalent to those of members with stirrups.

Mitchell, D et al. [22] built five large-scale reinforced concrete columns and wall boundary elements to observe the confinement performance provided by the headed transverse reinforcement. The results of the experiment showed that the specimens with the headed bar as the confinement reinforcement provided a performance similar to that of the specimens using hoop and crossties.

Kim, Y.H et al. [23] conducted an experimental test on specimens representing a heavily reinforced concrete portion of a wall structure. Specimens with 900 stirrup could not acquire strain above yielding due to the anchorage loss caused by splitting and concrete crushing. Interestingly, specimens with double headed stirrup could reach strain hardening.

A significant amount of research on the self-consolidating concrete (SCC) technology has been devoted to evaluating the suitability of the material for its use in structural applications. However, more research is required to confirm the adequacy of SCC structural members for resisting gravity and seismic loads. Mobin, J.S et al. [24] experimentally investigated the seismic performance of interior reinforced concrete beam-column connections with SCC. Four beam-column connection specimens, three with SCC and one with the normally vibrated concrete (NC), were designed for this experimental study. The performance of SCC specimens was comparable with that of NC specimens in terms of strength, displacement and ductility, but SCC specimens showed a lower energy dissipation capacity.

SCC is characterized by its high filling capacity due to its high viscoplastic deformability and also, its ability to maintain a stable composition throughout transportation and placing. SCC is a highly fluid concrete that can be easily placed and consolidated under its own weight to fill formwork, even in sections with highly congested reinforcement. Faster pouring and construction, better surface finishes, and a low noise level on the construction site are some of the advantages of SCC [25].

In a series of experiments conducted by Dhakal et al. [26] at the University of Canterbury, New Zealand, the seismic behavior of beam-column joints with the self-consolidating concrete under reversed cyclic load was investigated. This study reported that the specimens with the normal concrete and those with the self-consolidating one generally had an identical seismic behavior, and using the latter did not compromise any critical parameters of the seismic performance. Hence, they suggested that the self-consolidating concrete could be a better option for areas with the highly congested reinforcement such as columns and joints in the reinforced concrete frame structures. Chien et al. [27] investigated the behavior of the self-consolidating concrete in two groups of columns, one consisting of 16 columns made with normal concrete and the other including 16 columns made with the self-consolidating concrete. This study reported that self-consolidating concrete specimens had about 15% higher stiffness and 32% higher ductility than the normal concrete ones, and that using this concrete resulted in 18% reduction in the width of the cracks.

According to the research conducted in the area of beam-column joints with headed bars and the limitations imposed in the part 25.4.4.1 of ACI318-14 [28] on the type of concrete, concrete shall be of the normal weight, and the relative head area, the net bearing area of head A_{brg} shall be at least $4A_b$; the present study, therefore, investigated the compliance of these types of joints with the seismic criteria given by ACI 318-14 [28] when (a) the joint was made with the self-consolidating concrete, and (b) the joint was designed with the relative head area (the ratio of net head area to the nominal bar area) of 3 instead of 4.

2. Experimental program

The tests were carried out on four interstory exterior beam-column connections: two connections made with the normal

concrete and the other two made with the self-consolidating concrete. The first specimen (JH1-NC) was built exactly as instructed in ACI318-14 [28]; the second specimen (JH2-SCC) was made with the self-consolidating concrete instead of the normal one; the third specimen (JH3-NC) was made with the normal concrete, but with the relative head area (A_{brg}/A_b) being reduced to 3, that is, 25% lower than that specified in ACI318-14; and finally, the fourth specimen (JH4-SCC) was made with the self-consolidating concrete, with A_{brg}/A_b being reduced to 3. These joint specimens were designed for a 4-story structure with the story height of 3.15 m, the span length of 5.00 m at both direction of the plan, the dead load of 6 kN/m^2, and the live load of 2 kN/m^2, with the assumption of being located in an area of moderate seismicity. All specimens were built at the $\frac{2}{3}$ scale.

3. Design of joint specimens

The specimens were designed in accordance with the seismic design requirements of ACI318-14 and the criteria specified in the section 25.4.4 of ACI318-14 [28], except when design parameter was the subject of study. The studied parameters were: (1) the type of concrete, which was changed from normal to self-consolidating (in the specimens JH2-SCC and JH4-SCC), and (2) the relative head area, which was reduced from the minimum value specified in the code, that is, $A_{brg}/A_S = 4$ to $A_{brg}/A_S = 3$ (in the specimens JH3-NC and JH4-SCC). The full details of the specimens are presented in Fig. 1. The specimens JH1-NC and JH2-SCC were designed in accordance with ACI 318-14 [28], and the specimens JH3-NC and JH4-SCC were designed with the reduced A_{brg}/A_b. All joint specimens consisted of a continuous column with a beam connected on one side.

In all specimens, the column had a length of 2.10 m and a 350 × 320 mm cross-section. The beam was 1.65 m long and had a rectangular cross-section with the width of 320 mm and the depth of 350 mm. The beams and columns of specimens were given reinforcements of identical size and pattern, except when a change was necessitated by the experimental design. In all joints, the compressive and tensile reinforcements were provided by three rebars 20 mm in diameter. All columns were reinforced by eight rebars 18 mm in diameter. In all specimens, the spacing of the longitudinal reinforcement in the beam and the column was not less than twice that of the bar diameter.

The flexural and shear strength requirements of the beams were satisfied according to ACI318-14 [28]. The nominal flexural strength of the cross section, after applying the overstrength factor of $\alpha = 1.25$ on f_y, M_n was calculated to be 146.93 kN·m.

To prevent shear failure in the joint before a hinge appeared at the beam, the nominal shear capacity, $V_n$on the horizontal plane within the joint was checked to be higher than the maximum joint shear demand, V_u.

To prevent the formation of flexural hinges in the column and provide the conditions for hinge formation in the beam, the flexural strength of the beams and columns connected to the joint need to satisfy the following condition:

$$\sum \frac{M_{\text{n-column's}}}{M_{\text{n-beam's}}} > 1.2 \quad (1)$$

After performing the calculations for the considered beam and column cross sections, the moment of resistance of the beam in the specimens with one row of reinforcement was obtained to be $M_r = 109.0\ \text{kN} \cdot \text{m}$, and the moment of resistance of each column connected to the joint was calculated to be $M_r = 126.30\ \text{kN} \cdot \text{m}$. Thus, the joint was found to satisfy the above condition.

According to the Section 25.4.4.2 of ACI318-14 [28], the anchorage length of the headed bars, L_{dt}, shall not be less than maximum of $0.19 f_y d_b \omega_e / \sqrt{fc}$, $8d_b$ and 150 mm.

For steel bars without epoxy coating, $\omega_e = 1$. Therefore, by having the size of the bars and the measured compressive strength of the normal and self-consolidating concretes and the measured yield strength of steel bars, the minimum required anchorage length and the final anchorage length used in the specimens were obtained, as shown in the following table (Table 1).

4. Materials of the joint specimens

The steel bars used in the specimens were of the same type. Both normal and self-consolidating concretes were designed to gain the strength of $f_c^{'} = 40$ MPa. At the time of casting specimens, the standard cylindrical samples were taken in three instances. These samples were subjected to the 28-day compression strength test and the average result was recorded as the characteristic strength of concrete. The actual strength of normal and self-consolidating concretes was found to be 40 MPa and 41 MPa, respectively. Table 2 shows the mix design of each type of concrete.

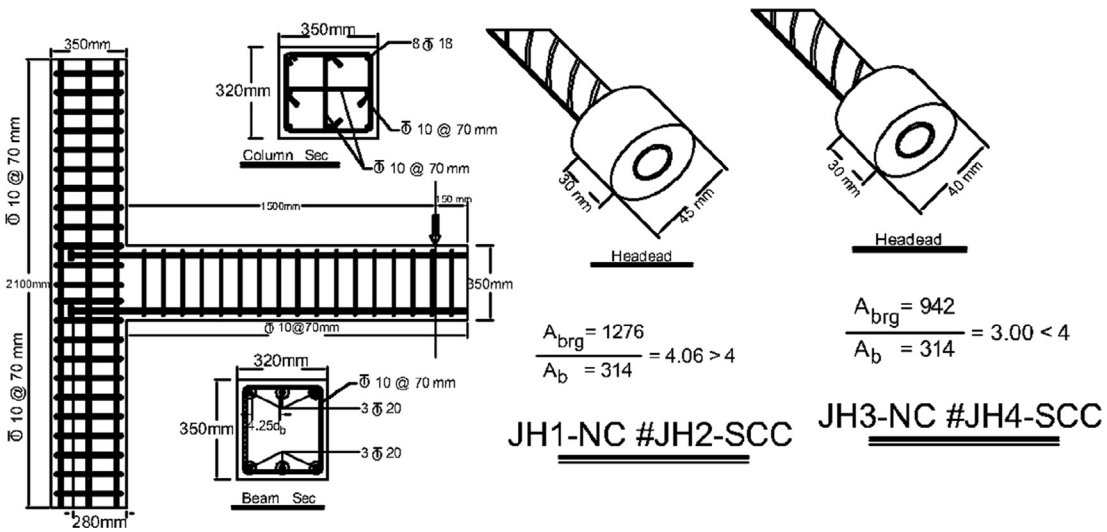

Fig. 1. Dimensions and details of the specimens and Heads and threaded connections.

Table 1
Anchorage length of the headed bars in the beam-column joint specimens.

Sample umber	Diameter of rebar (mm)	$f_c^{'}$ (MPa)	f_y (MPa)	Min L_{dt} (mm)	Using L_{dt} (mm)
JH1-NC	20	40	442	265	280
JH2-SCC	20	41	442	262	280
JH3-NC	20	40	442	265	280
JH4-SCC	20	41	442	262	280

Table 2
Mix design of concretes used in the joint specimens.

Materials and parameters	Unit	Normal concrete	Self-consolidating concrete
Cement	$\frac{Kg}{m^3}$	360	355
Sand	$\frac{Kg}{m^3}$	1050	1084
Gravel	$\frac{Kg}{m^3}$	810	610
$\frac{w}{c}$	–	0.45	0.45
Superplasticizer	$\frac{L}{m^3}$	1.5	3.50
Microsilica	$\frac{Kg}{m^3}$	–	65
Slump	mm	80	–
Slump flow diameter	mm	–	640
V-Funnel test	Sec	–	6

Tensile strength of the steel bars was determined based on ASTM A-370 [29] guidelines. The average mechanical properties obtained from these tests are presented in Table 3.

5. Test apparatus

Joint specimens were constructed at the $\frac{2}{3}$ scale. Beams had a length of 1.65 m, and columns had a total height of 2.10 m. The specimens were tested in the horizontal orientation with the two ends of the column being considered to have the roller support with free rotation and the constrained lateral displacement. The horizontal displacement of the upper end of the beam, which was needed for plotting the force-displacement curve, was measured by attaching Linear Variable Displacement Transducers (LVDTs) to this section. Figs. 2 and 3 display the images of the test apparatus, the placement of the specimens, equipment, strain gauges and the loading frame.

The pseudo-static cyclic lateral load was applied (Fig. 4), according to a previously defined loading history to the upper end of the beam based on ACI 374-2005 guidelines [12]. The test apparatus had a loading capacity of 600 kN and could apply 90 mm displacement (in both directions) to the upper end of the beam by the displacement-control technique. By using a hydraulic jack, the column head was subjected to a constant axial load with a magnitude of 140 kN and was controlled to remain constant in all loading cycles; when needed, corrections were made to compensate for the effect of deformations on the force.

The displacement transducer used in this study was able to measure the displacements of up to 200 mm in each directions. The device was installed so that it could measure the displacement of the beam in both directions, and it was connected to a data logger via a cable. The data obtained from the transducer was used to plot load-displacement curves. The load applied to the specimen was measured by an S-shaped force meter capable of measuring tensile and compressive forces of up to 200 kN. The measurements of this force meter were also recorded in a data logger. All data including the loads recorded by the force meter, oil pressure during tensile and compressive loading, and displacement of the end of the beam were recorded and then exported to a computer. In the computer, the load-displacement curves were plotted with the software dedicated to the processing of the above information.

6. Analysis of test results

The diagram of load versus displacement over the course of loading cycles is the best means for the accurate evaluation of the joint performance under cyclic loadings. This diagram allows us to determine some key parameters such as the time of final failure, ductility capacity, and energy absorption of the specimen, as well as judging the joint performance. The horizontal axis of the hysteresis curve represented the displacement in millimeters and the corresponding drift and its vertical axis showed the applied load in kilonewtons. By having the distance between the load point (at the beam) and the joint face (at the column), which was 1.5 m in this study, the bending moment of the beam at the joint face could be calculated.

6.1. Behavior of the normal and self-consolidating concrete specimens

Fig. 5 displays the load-displacement diagram of the normal concrete (JH1-NC) and self-consolidating concrete (JH2-SCC) specimens. These joints were designed according to the criteria cited in the section 25.4.4.2 of ACI318-14 [28] to be used as the control and ideal specimens. Having built in compliance with ACI318-14 [28] criteria, these joint specimens were expected to fail by the formation of a plastic hinge in the beam. As shown in the hysteresis diagrams (Fig. 5), with the increase in the displacement of both positive and negative directions, the applied load was raised, and the load drop was not observed until the drift of 5.5%. In the specimen JH1-NC, the first crack, which was of the bending type, appeared in the beam at the beam-column interface with 0.58% drift and 31.20Having built in compliance kN force. After reversing the loading direction, similar cracks appeared on the other face of the beam. These cracks, which were also of the bending type, were formed before the reinforcements yield. According to the hysteresis curve of this specimen, the maximum bearing capacity of this joint was $P_{peak} = 101.75$ kN, which corresponded to the relative displacement of $\delta_{peak} = 34.50$ mm at DR = 4.05%. The corresponding moment, 152.63 kN·m, was larger than the bending capacity of

Table 3
Measured Mechanical properties of the longitudinal and transverse reinforcement bars used in the Experiment.

Rebar diameter (mm)	f_y(MPa)	f_u(MPa)	*ε_y (%)	*ε_u (%)	$E = \frac{f_y}{\varepsilon_y}$ (MPa)
10	436	674	0.002	15.95	218,131
18	466	665	0.002	16.18	233,140
20	442	653	0.002	15.98	221,133

* From the rebar tension test diagram.

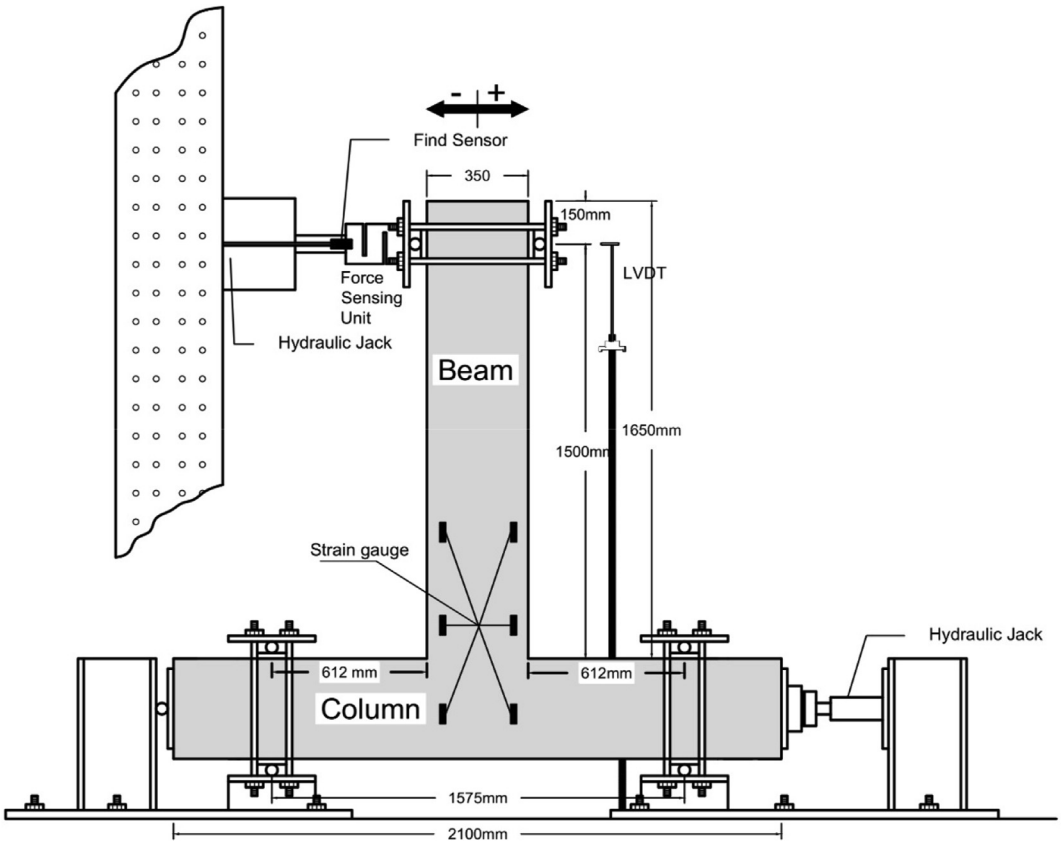

Fig. 2. Test apparatus.

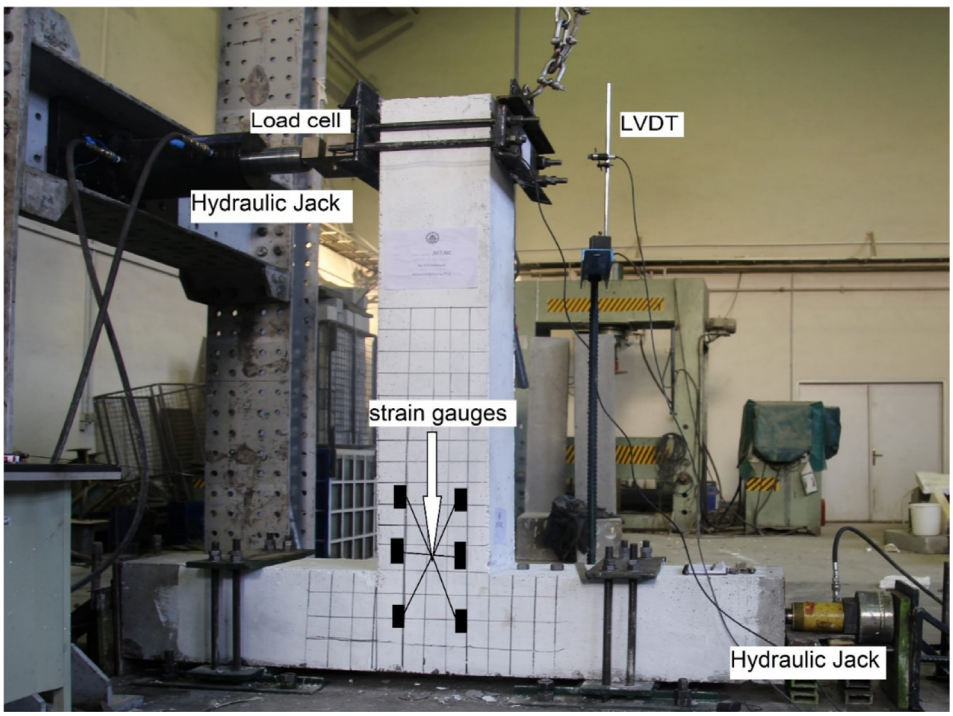

Fig. 3. Loading frame.

the section of the beam (M_P), which, according to the principles of analysis of beams for bending based on the nonlinear distribution of stress and the linear distribution of strain, was 146.93 kN·m. The displacement corresponding to the yield of longitudinal bars in the beam was $\delta_y = 11.16$ mm, which occurred at DR $= 0.77\%$ and corresponded to $P_y = 42.25$ kN. These data were obtained from the

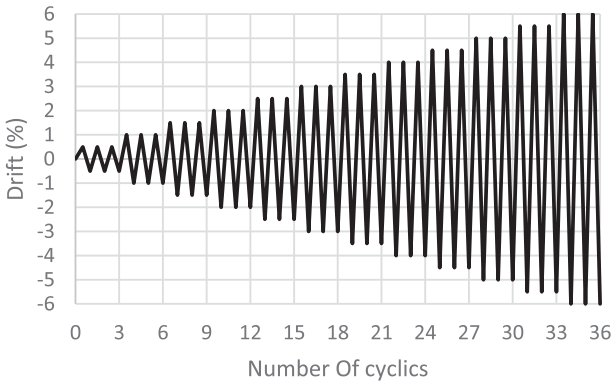

Fig. 4. Loading history used in the test.

strain gauges of the longitudinal bars. As the bending cracks were appeared in the beam, the joint core started to develop diagonal cracks. This was continued until the load of P_y, above which new cracks were mostly diagonal cracks emerging in the joint core, and very few bending cracks were formed in the beam (Fig. 6). Given the cyclic nature of loading, cracking in the joint core was inevitable. In this specimen, crushing started in the beam-column interface at the 4% drift and peaked at the 6% drift.

The specimen JH2-SCC behaved generally similarly to JH1-NC. In this specimen too, the first crack was of the bending type and appeared in the interface of the beam with the column at the 0.51% drift and the 40.82 kN force. With the change in the loading direction, similar bending cracks appeared on the other face of the beam before the reinforcements yield. The hysteresis curve of this specimen showed that the maximum bearing capacity of the joint was $P_{peak} = 104.12$ kN, which corresponded to the relative

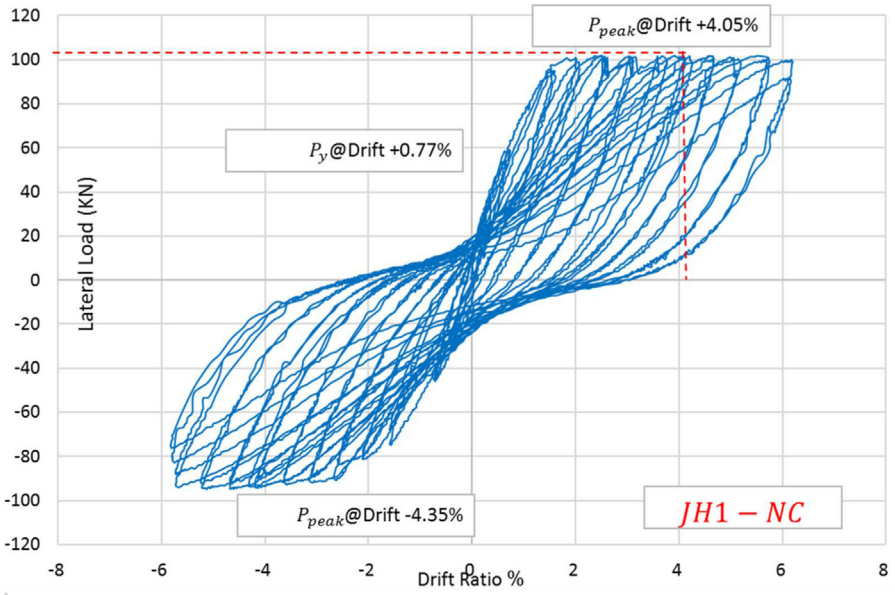

(a) JH1-NC

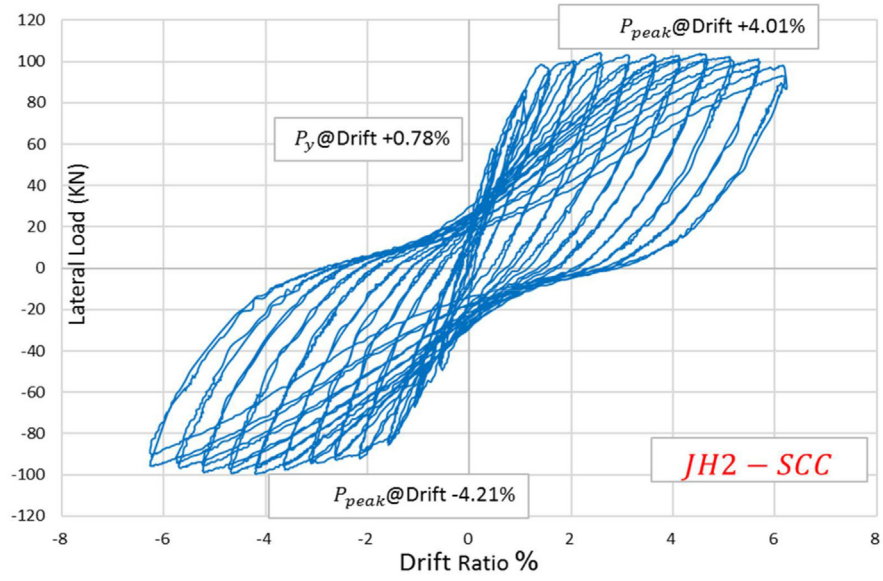

(b) JH2-SCC

Fig. 5. Load-displacement diagram of the specimens JH1-NC and JH2-SCC.

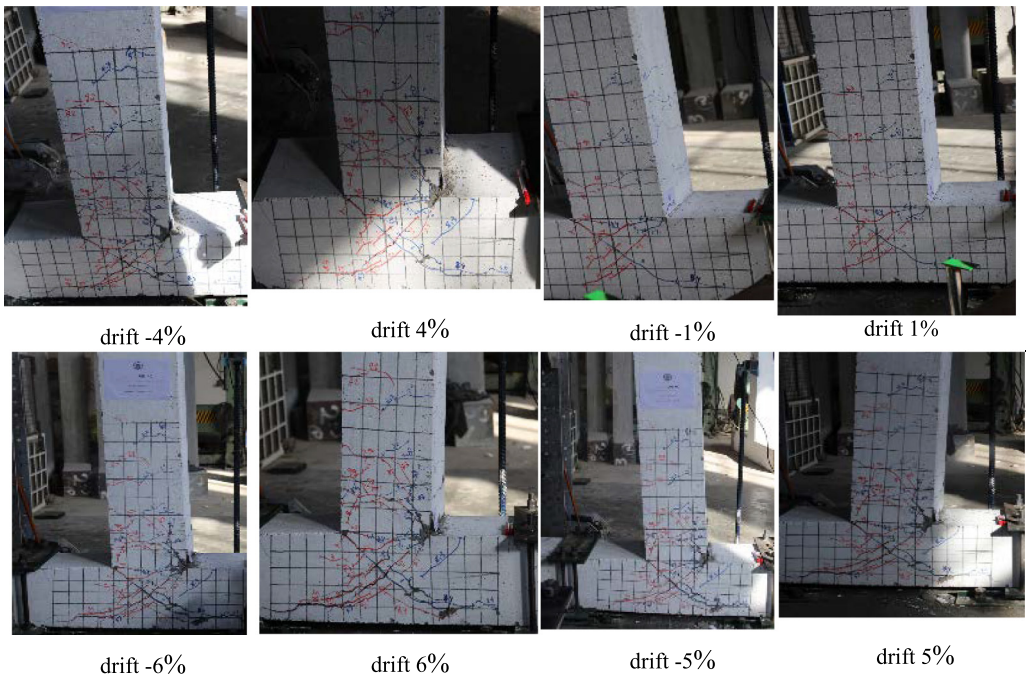

Fig. 6. Crack propagation under loading in the specimen JH1-NC.

displacement of $\delta_{peak} = 29.80$ mm at DR = 4.01%. As before, the corresponding moment, 156.18 kN·m, exceeded the bending capacity of the beam section (M_P), which was 147.23 kN·m. The displacement corresponding to the yield of the longitudinal bars of the beam was $\delta_y = 11.40$ mm, which occurred at DR = 0.78% and corresponded to $P_y = 45.82$ kN. The crushing of this specimen also started at the 4% drift and peaked at the 6% drift. This specimen showed 2.33% higher bending capacity and a better seismic behavior than JH1-NC. As expected, the curve of these specimens generally had a taller and wider extension than the previous one. These changes could be attributed to the use of the self-consolidating concrete (SCC) instead of the normal concrete (NC), indicating the greater energy absorption potential of SCC rather than NC. This is because SCC has more adhesion to the bars, resulting in the higher resistance to detachment. It also has a higher amount of superplasticizer, giving better fluidity and resulting in better placement around corners and between the reinforcement bars. The hysteresis curves of Fig. 5 do not show any pinching effect (narrowing of the middle part of hysteresis loops), suggesting that the joint could absorb or damp the energy until the moment of failure. This is, in fact, one of the important features deciding how a structure performs under the seismic load.

The pattern of crack propagation in the specimens JH1-NC and JH2-SCC during loading at different drifts is shown in Figs. 6 and 7, respectively.

6.2. Behavior of the specimens with a reduced relative head area

Fig. 8 illustrates the load-displacement diagram of the joint specimens JH3-NC and JH4-SCC. These hysteresis diagrams show that in the specimen made with the self-consolidating concrete, with the increase in displacement in both positive and negative directions, the applied load was increased, and the load drop was not observed until the 5.75% drift. In the specimen made with the normal concrete, a similar trend was observed in the negative direction, but the load drop in the positive direction started at the 4.7% drift.

In the specimen JH3-NC, the first crack, which was, again, of the bending type, emerged in the beam at the beam-column interface at the 0.54% drift and the 40.36 kN force. Then, other bending cracks emerged on the other face of the beam before the reinforcements yield. The maximum bearing capacity of this joint specimen was $P_{peak} = 102.25$ kN, which corresponded to the relative displacement of $\delta_{peak} = 26.00$ mm at DR = 3.01%. The corresponding moment was 153.63 kN·m, which was larger than the bending capacity of the section, that was, 146.93 kN·m. The displacement corresponding to the yield of the longitudinal bars of the beam was $\delta_y = 11.12$ mm, which occurred at DR = 0.77% and corresponded to $P_y = 39.50$ kN. Before reaching the load of P_y, this specimen showed bending cracks in the beam as well as diagonal cracks in the joint core. However, after P_y, new cracks mostly appeared at the side of the joint. This suggested that plastic hinge was directed toward the length of the beam. Nevertheless, the specimen also developed some diagonal cracks in this stage. The crushing of this specimen started at the 4% drift and peaked at the 6% drift.

Likewise, the first crack of the specimen JH4-SCC was of the bending type and it was formed in the beam in the point where it met the column at the 0.59% drift and the 44.38 kN force. Other bending cracks then appeared on the other face of the beam before the reinforcements yield. The maximum bearing capacity of this specimen was $P_{peak} = 104.79$ kN, which corresponded to the relative displacement of $\delta_{peak} = 29.70$ mm at DR = 3.96%. The corresponding moment was 157.19 kN·m, which was greater than the bending capacity of the section, that was 147.23 kN·m. The displacement corresponding to the yield of the longitudinal bars in the beam was $\delta_y = 10.56$ mm, which occurred at DR = 0.79% and corresponded to $P_y = 34.49$ kN. After comparing the results of these two specimens, it was found that the specimen made with the normal concrete and a reduced relative head area had 0.50% higher flexural capacity than the control specimen, which suggested that the change made in this specimen was indeed permissible. Also, the specimen made with SCC and the reduced relative head area showed 3% higher flexural capacity than the control specimen and 2.49% higher flexural capacity than the specimen

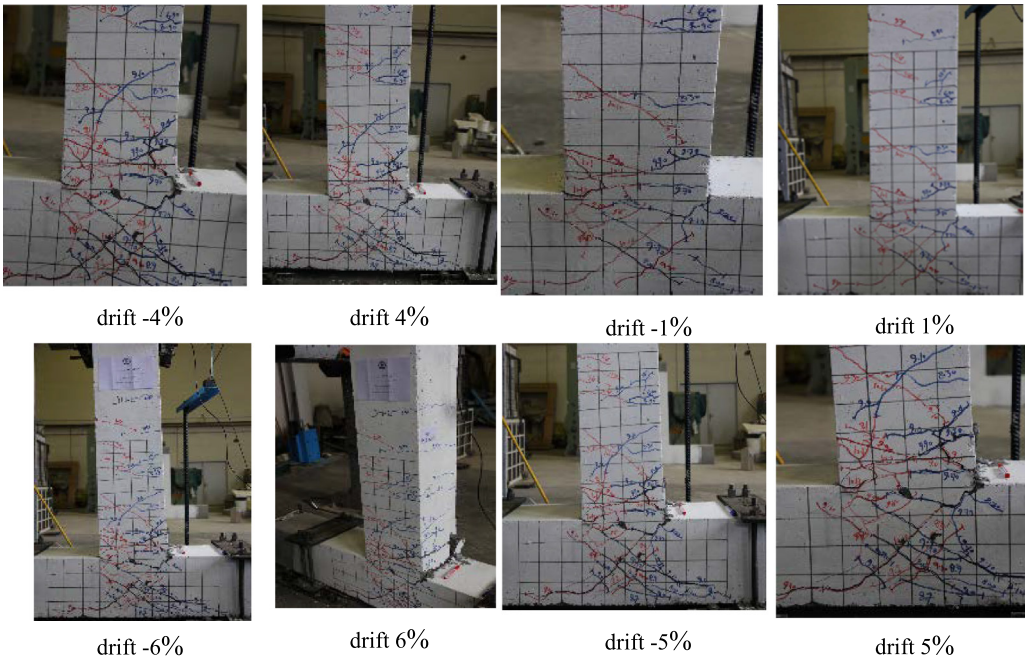

Fig. 7. Crack propagation under loading in the specimen JH2-SCC.

JH3-NC. This improvement could be attributed to the effect of using headed bars with a lower relative head area. According to the area below the hysteresis curve, the last specimen also had a better seismic behavior, which, again, supported the value of using headed bars with the lower relative head area together with the self-consolidating concrete. Also, these hysteresis curves did not show the pinching effect and had a greater area under the curve in comparison to the control specimen. According to these results, this joint could be expected to exhibit excellent capability in absorbing or damping the energy until the moment of failure; a capability that, as mentioned earlier, plays a key role in how a structure behaves under a seismic load.

Figs. 9 and 10, show the pattern of crack propagation in the specimens JH3-NC and JH4-SCC at different drifts.

6.3. Joint efficiency, load-bearing capacity and ductility

Joint efficiency is a key parameter in the analysis of joints. Joint efficiency (Z) is defined as the ratio of the ultimate moment of the resistance of the joint to the plastic moment of the beam or $Z = \frac{M_u}{M_P}$, where M_u is the moment endured by the entire joint including beam and column and can be obtained from the experiment, and $M_P$is the moment capacity of the beam, which can be calculated according to the principles of analysis of beams for bending based on the nonlinear distribution of stress and the linear distribution of strain over the section height. From a structural perspective, a joint is called efficient when it has satisfactory rotation capacity as well as 100% or more efficiency. By allowing stress and moment redistribution at the core, such a joint is able to withstand the moment applied on the frame even after the formation of a plastic hinge in the beam. By having the geometric dimensions and the area of the beam reinforcements, M_P of each specimen was calculated and then divided by the moment arm (the distance between the column and the load point) to calculateP_P. The results of this calculation and the obtained efficiency values are presented in the Table 4. As can be seen, the obtained Z values were all greater than 100%, which suggested that the joints were permissible from the efficiency perspective. In ACI 374-2005 [9], the failure criterion is the point where the load reaches 75% of the maximum bearing capacity, and the joint is acceptably efficient against the seismic load when the failure occurs at the drifts of more than 3.5%. In all of the load-displacement curves obtained in this study, the decrease in the maximum capacity with the increase in drift was negligible, and none of the maximum points of the curves, including those related to the drifts of less than 3.5%, was less than $0.75P_{peak}$. It could, therefore, be concluded that all joint specimens enjoyed the satisfactory efficiency.

Ductility of members is a key parameter in designing RC structures for earthquake-prone areas. In this study, ductility refers to the displacement as expressed by the relation $\mu_d = \frac{\delta peak}{\delta y}$; here, δ_y is the displacement at the first point where the steel yields and δ_{peak} is the displacement related to the maximum load-bearing capacity of the joint [27]. The ductility values calculated based on the columns 3 and 5 of Table 4 are presented in the column 8 of the same table.

6.4. The effect of the concrete type on the results

One of the main objectives of this study was to investigate the effect of the replacement of the normal concrete with the self-consolidating one in the joins with headed bars. Thus, to assess the possibility of using the self-consolidating concrete in these joints, this section compares the results of the specimens JH1-NC and JH2-SCC, which were both designed according to ACI criteria, with the second one representing the self-consolidating concrete instead of the normal one. Here, the specimen JH1-NC, which was made exactly as specified in ACI, was considered as the control specimen. The results of Table 4, the hysteresis curves of Fig. 5, and the cracks observed in these two specimens suggested that using the self-consolidating concrete instead of the normal concrete increased the efficiency of the joint structure. As shown in Table 4, the joint specimen JH2-SCC had the efficiency of 1.06, which was about 2% better than that of the specimen JH1-NC, that was 1.04. According to the hysteresis curves of these two specimens (Fig. 5) and the column 1 of Table 4, the specimen JH2-SCC also had 2.33% higher capacity than JH1-NC. The joint failure mecha-

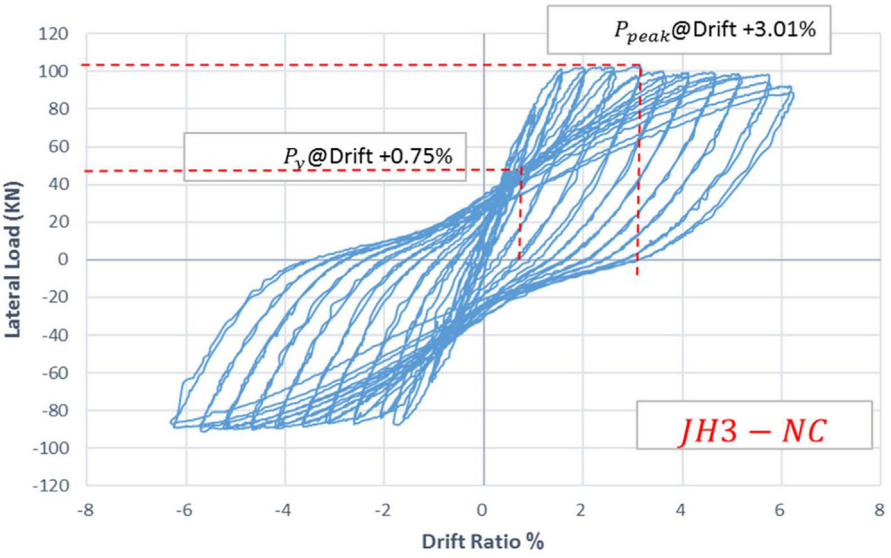

(a) JH3-NC

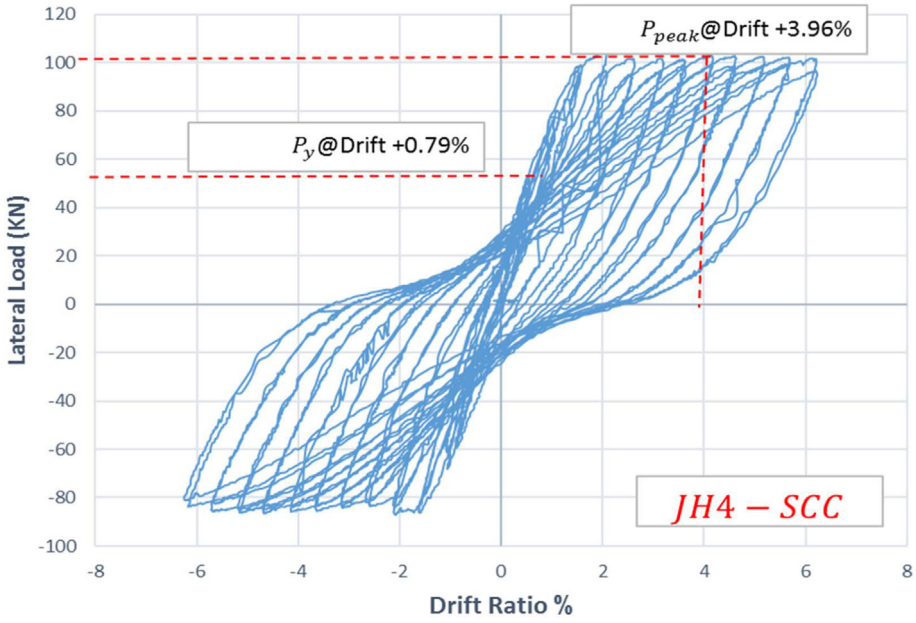

(b) JH4-SCC

Fig. 8. Load-displacement diagram of the specimens JH3-NC and JH4-SCC.

nism was also investigated by examining the cracking patterns. This investigation revealed the development of significant bending cracks with limited damage in the beam-column interface of the specimen JH1-NC during the 1.50% drift cycle and in the same area, in the specimen JH2-SCC during 1.00% to 1.50% drift cycles. At drifts of about 3.50%, the cracks of both specimens started to propagate from the interface into the beam, eventually progressing as much as half of the beam height into the specimen JH1-NC and as much as the entire beam height into the specimen JH2-SCC. This suggested that, in both specimens, the plastic hinge had been formed in the beam, but in JH2-SCC, this plastic hinge was located farther away from the joint interface. In both specimens, diagonal cracks stopped appearing in the joint core; this is a pattern that could be attributed to the cyclic nature of loading. After measuring the width of the cracks at the end of the loading cycles, it was found that the cracks formed in the self-consolidating concrete were about 16% less wide than those in the normal one. This indicated that, as expected, the self-consolidating concrete had better adhesion to the reinforcement bars. From the push over load-displacement curves of two specimens, it was determined that the specimen made with the self-consolidating concrete had a higher load-bearing capacity than the one made with the normal concrete, while the load drop in both specimens started from about the same drift (Fig. 11). Thus, after examining the parameters that affected the joint performance, it was concluded that the specimen made with the self-consolidating concrete was not weaker; in fact, it was much better than the control specimen. It can, therefore, be stated that the ACI criteria for the design of joints with headed bars and normal concrete can also be used for the design with the self-consolidating concrete.

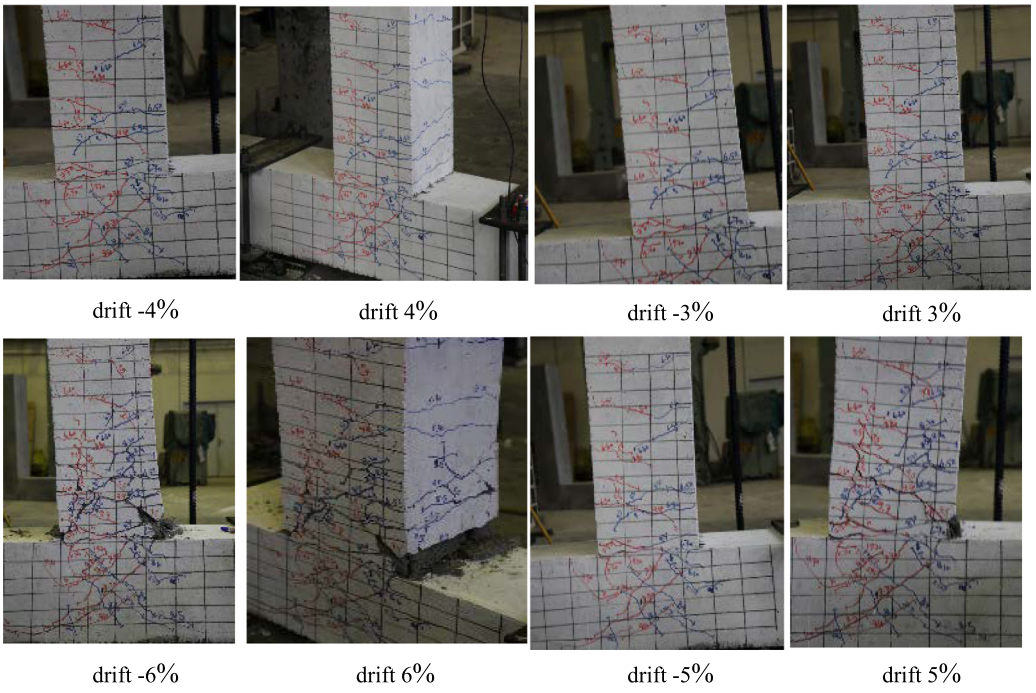

Fig. 9. Crack propagation under loading in the specimen JH3-NC.

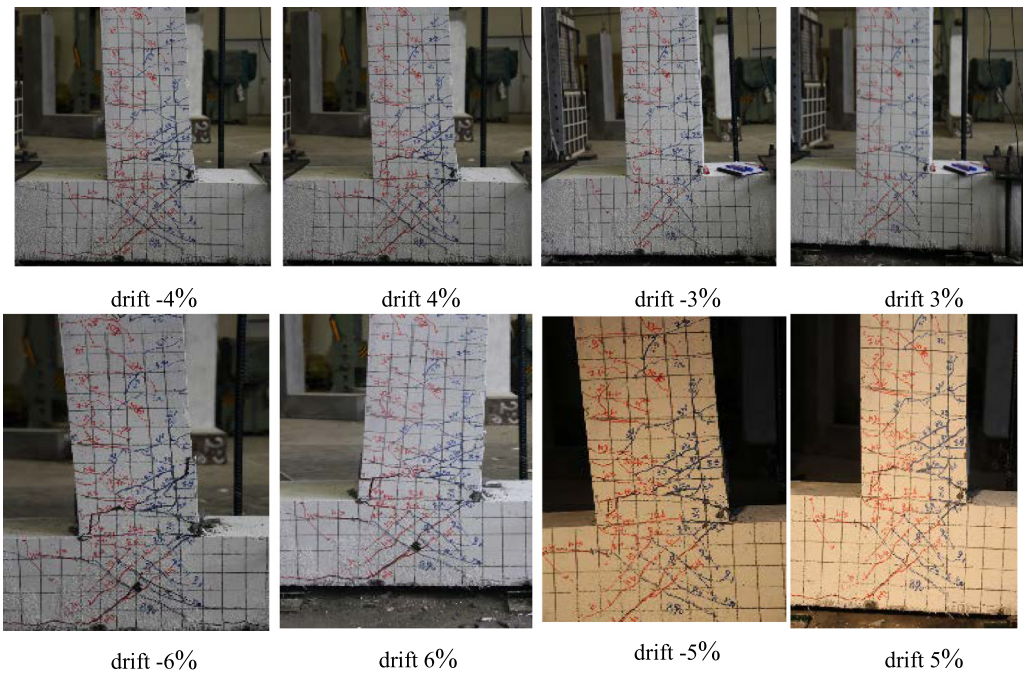

Fig. 10. Crack propagation under loading in the specimen JH4-SCC.

Table 4
Summary of the results of the experiments and the related calculations.

Sample number	P_{peak} (kN)	δ_{peak} %))	P_y (kN)	δ_y (%)	P_P (kN)	$^*Z = \frac{P_{peak}}{P_p}$	$\mu_d = \frac{\delta_{peak}}{\delta_y}$
JH1-NC	101.75	4.05	42.25	0.77	97.95	1.04	5.26
JH2-SCC	104.12	4.01	45.82	0.78	98.15	1.06	5.14
JH3-NC	102.25	3.01	39.50	0.77	97.95	1.04	3.91
JH4-SCC	104.79	3.96	34.49	0.79	98.15	1.06	5.01

$^*Z = M_u/M_p = (P_{peak} \cdot l_b)/(P_p \cdot l_b) = P_{peak}/P_p$.

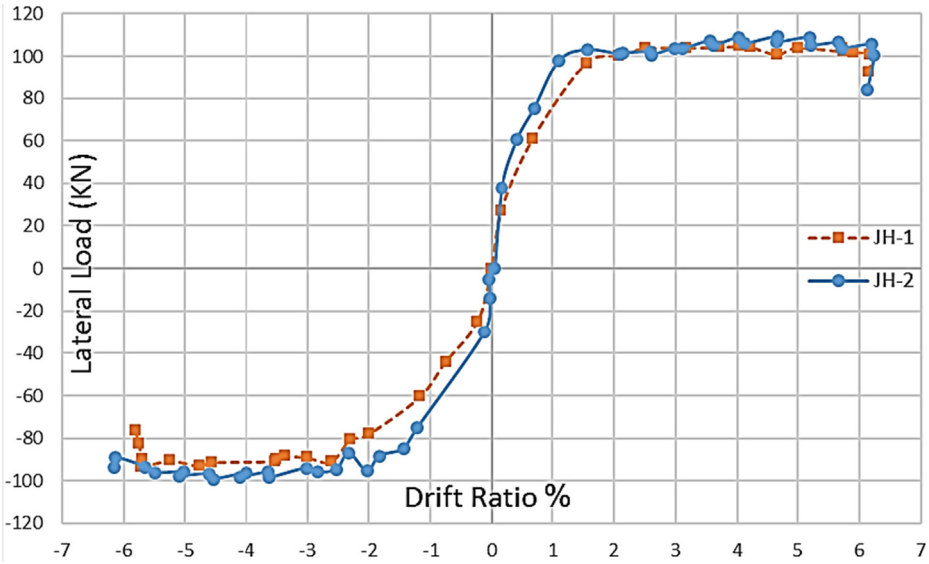

Fig. 11. Backbone curves of the specimens JH1-NC and JH2-SCC.

6.5. The effect of the reduced relative head area

According to the results of Table 4, reducing the relative head area from $A_{brg}/A_S = 4$ in the specimen JH1-NC to $A_{brg}/A_S = 3$ in the specimen JH3-NC did not reduce the joint efficiency (Z = 1.04). Thus, the latter specimen was permissible in terms of efficiency. Also, according to the maximum capacity values presented in the column 2 of this table, this change led to a very slight improvement in the load capacity (about 0.5%). The hysteresis curve of the specimen JH3-NC (Fig. 8) did not exhibit the pinching effect; in fact, it had a greater area under the curve than the hysteresis curve of the control specimen. Thus, it could be claimed that this specimen had a desirably more ductile behavior than the control specimen. In terms of strength degradation against lateral load, the specimen JH3-NC behaved somewhat similarly to the control specimen, as strength degradation started at the 2.55% drift and there was no sharp drop in drift until the end of the loading cycle. Also, none of the maximum points of the curves, including those related to the drifts of less than 3.5%, were less than 0.75 P_{peak}, so the joint satisfied this seismic requirement as well. The patterns of crack development during the experiment and the final cracks at the end of the loading (Fig. 13) pointed to the formation of a ductile hinge in the beam in the area near the column and its growth until the drift of 5.1%. However, in the final loading cycles, the shear cracks were grown widely and the concrete near the joint face was significantly crushed. Another observation was the reduced bending strength in the high drifts, which was due to the slip of the longitudinal bars of the beam. The substantial crushing of concrete on the sides began at a drift of 4.25% and reached a maximum level at the end of loading. One of the interesting observations made in this joint was the insignificant propagation of diagonal cracks in the joint core, which only slightly grew widely

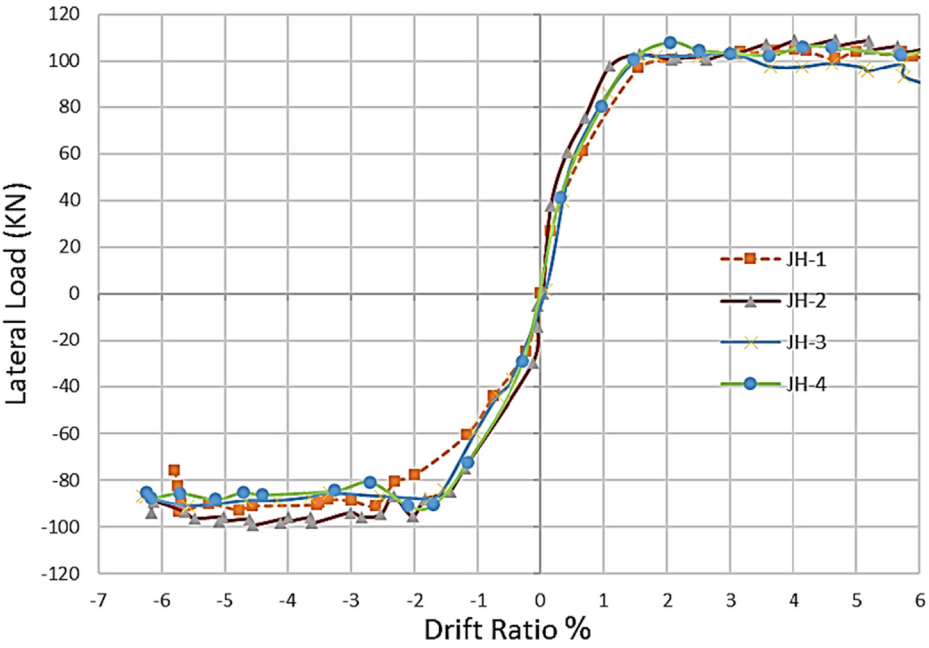

Fig. 12. Backbone Curves of the specimens JH1-NC, JH2-SCC, JH3-NC and JH4-SCC.

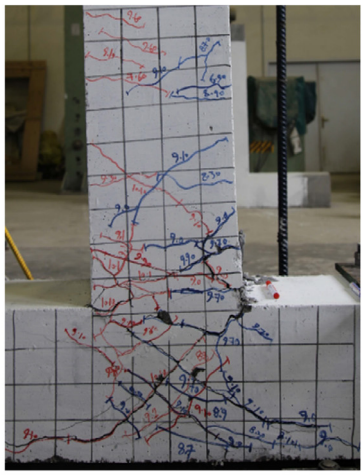

JH2-SCC

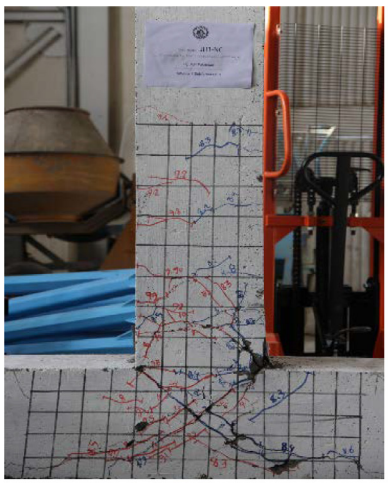

JH1-NC

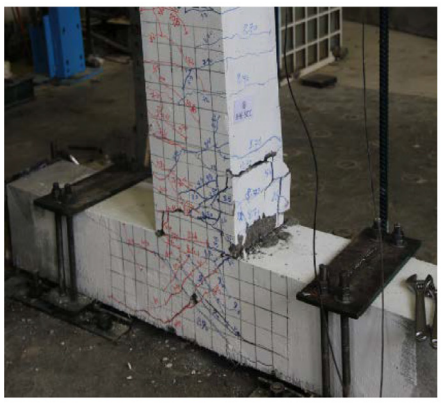

JH4-SCC

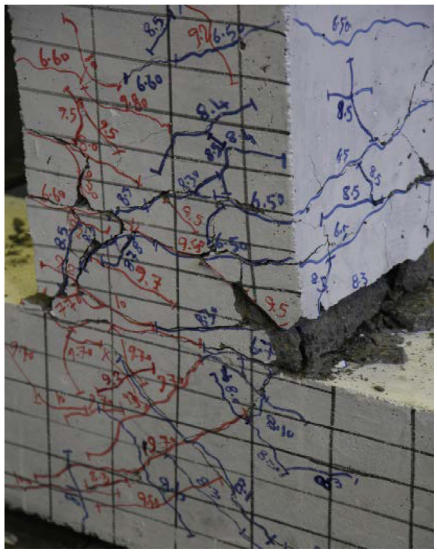

JH3-NC

Fig. 13. Cracking patterns at the end of the loading.

during the loading. This ensured that the formation of the hinge outside the joint core was more than what was found for the control specimen. As in JH1-NC, significant bending cracks with limited damage were observed at the beam-column interface during the 1.50% drift cycle. In the drifts of about 3.75%, these cracks were propagated from the joint face into the beam, ultimately progressing as much as half of the beam height. It should be noted that separate wider cracks appeared farther away from the joint face at a distance even greater than the beam height. According to the push over load-displacement diagrams, although the load drop in these specimens started from about the same drift, the specimen JH3-NC had a slightly higher maximum bearing capacity than the control specimen (Fig. 12). Hence, given the above results and the ductile behavior of the specimen JH3-NC, by considering the fact that it developed a plastic hinge in the beam and did not show any significant lateral strength degradation, especially in the drifts of less

Table 5
Assessment of the compliance of the joint specimens with the acceptance criteria of ACI 374-2005 [9].

Sample umber		P_{max} (kN)	P_{3rd} (kN)	$\frac{P_{3rd}}{P_{max}}$	θ'_1	θ'_2	A_h	β
JH1-NC	+	101.75	101.55	0.998	2.86	2.84	314.55	0.2868
	–	94.74	90.89	0.959				
JH2-SCC	+	104.12	98.92	0.950	2.99	3.01	311.61	0.2701
	–	95.42	93.36	0.978				
JH3-NC	+	102.25	100.16	0.980	2.97	3.01	322.02	0.2850
	–	91.4	88.76	0.971				
JH4-SCC	+	104.79	98.97	0.944	2.96	2.99	325.01	0.2997
	–	86.91	83.3	0.958				

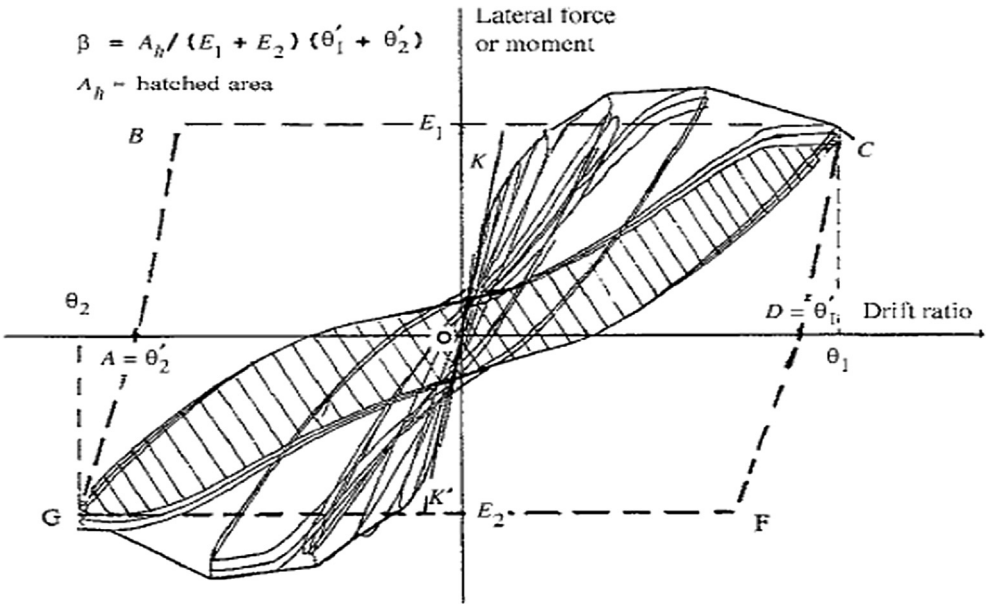

Fig. 14. Hysteresis curve and relationships for checking the compliance with the acceptance criteria of ACI 374-2005 [9].

than 4.0%, it could be concluded that the anchorage requirements of the joints with headed bars could be satisfied with a relative head area of about 3.

Using the self-consolidating concrete in the joint with the reduced relative head area (the specimen JH4-SCC) led to even better joint efficiency (Z = 1.07) in comparison to the control specimen (JH1-NC). This result demonstrated the permissibility of this specimen in terms of efficiency. According to Table 4, this specimen also had about 3% better bearing capacity than the control specimen. The hysteresis curve of this specimen did not show the pinching effect and had a greater area under the curve, as compared with the control specimen. Thus, it could be claimed that this specimen exhibited a better ductility behavior than the control specimen. In terms of the lateral strength degradation, a slight degradation started at the 2.25% drift, but there was no load drop until final drifts at the end of the loading cycle. Also, none of the maximum

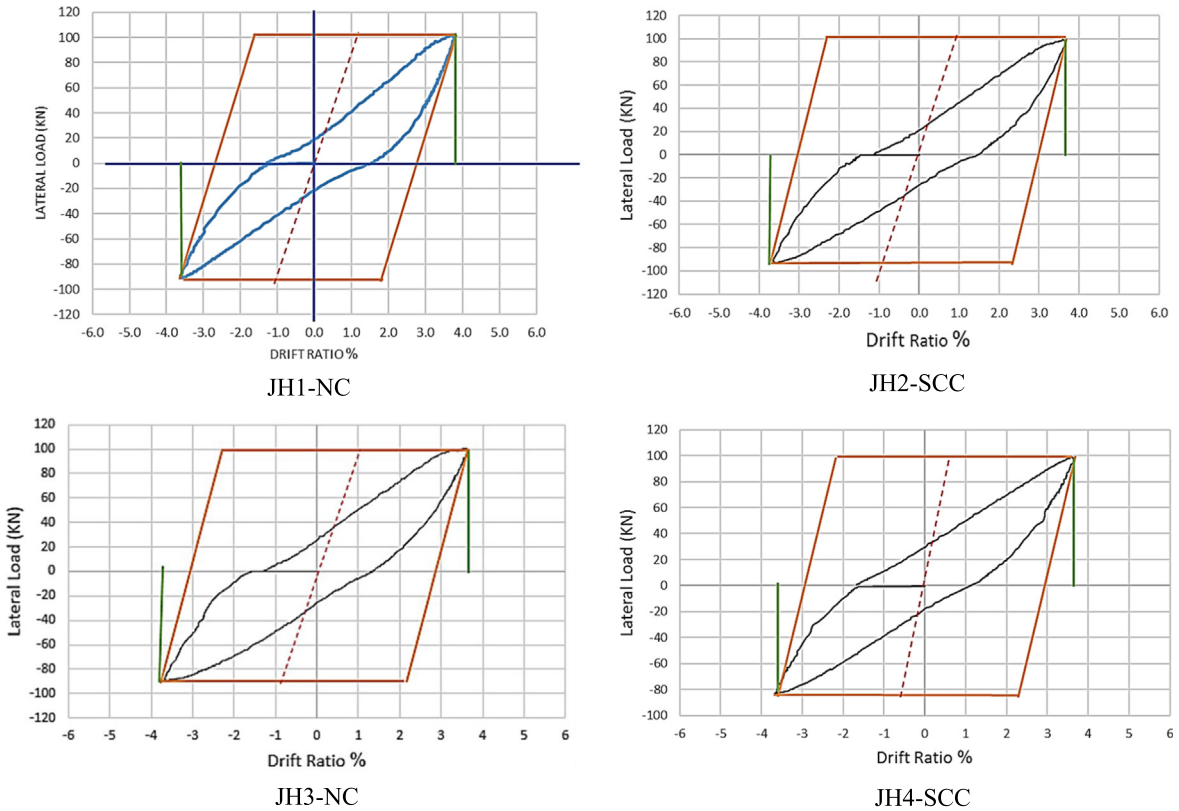

Fig. 15. The hysteresis curve is 3.5% for each connection.

points of the curves, including those related to the drifts of less than 3.5%, were less than $0.75P_{peak}$, so the joint satisfied this seismic requirement. From these results, it could be concluded that the anchorage requirements of the joints with headed bars could be satisfied with the relative head area of about 3 even when using self-consolidating concrete instead of the normal one.

6.6. Compliance with the acceptance criteria of ACI 374-2005

In ACI 374-2005 [9], the failure criterion for a joint is the point where the load reaches 75% of the maximum bearing capacity. According to this code, laboratory specimens should be able to satisfy the following requirements in the third cycle of the 3.5% drift:

(A) The maximum force resulting from loading shall not be less than 75% of the maximum force obtained during the experiment; in other words, $P_{3rd} \geq 0.75P_{max}$.
(B) The relative energy dissipation ratio (β), given by the equation coming below, shall not be less than 0.125.

$$\beta = \frac{A_h}{(\theta_1' + \theta_2')(E_2 + E_1)}, \quad \theta_1' = 0.35 - \frac{E_1}{hK_{in}^{+}} \quad \text{and} \quad \theta_2' = 0.35 - \frac{E_2}{hK_{in}^{-}} \tag{2}$$

In the above equation, A_h is the area within the hysteresis curve of the 3.5% drift, E_1 and E_2 are the magnitude of the maximum positive and negative force in the 3.5% drift, and $K_{in}^{\pm}$ is the initial stiffness along the positive and negative loading direction. The value of θ' and A_h can be obtained, as shown in Fig. 13, from the geometry of the hysteresis curve. In this study, θ' and A_h were determined by plotting the hysteresis curve of the 3.5% drift in the software AutoCAD.

Table 5 presents a summary of calculations performed using the discussed results and the hysteresis curve obtained for the 3.5% drift (Fig. 14) in order to control compliance with the above acceptance criteria. As indicated in this table, all joint specimens of this study could satisfy the requirements of the relevant code.

According to the results presented in the column 4 of Table 5, in all specimens, the maximum force resulting from the loading in the final cycle of the 3.5% drift was less than 75% of the maximum force obtained during the experiment (Fig. 15), implying that the condition $P_{3rd} \geq 0.75P_{max}$ was satisfied. In the column 8 of this table, it could be seen that the relative energy dissipation ratio (β) of all specimens was greater than 0.125, which means that they all met this requirement of the code as well.

7. Conclusions

The present study investigated the applicability of designing interstory exterior beam-column joints with header bars and self-consolidating concrete, using a lower relative head area (for headed reinforcements) than that recommended in the section 25.4.4.2 of ACI318-14 [28]. For this purpose, the researchers built four $\frac{2}{3}$ scale experimental specimens in two groups: two specimens with the normal concrete and the other two with the self-consolidating concrete. In each group, one specimen was designed with the recommended relative head area and another one was one using a 25% lower relative head area. All specimens were subjected to a pseudo-static cyclic load to investigate their compliance with seismic requirements in two conditions: (a) when using self-consolidating concrete instead of the normal one, and (b) when designing the headed longitudinal bars of the beam with the relative head area of $\frac{A_{brg}}{A_b} = 3$ instead of 4. The results of this study could be summarized as follows:

1. Using the self-consolidating concrete instead of the normal one in the joints with headed bars improved the joint efficiency and the bearing capacity. According to the crack width measurement made at the end of the loading cycles, the cracks that emerged in the self-consolidating concrete were 16% less wide than those appeared in the normal concrete. This indicated that, as expected, the self-consolidating concrete had better adhesion to the reinforcement bars. The specimen made with the self-consolidating concrete showed 2.40% higher ultimate load capacity than that of the control one. Hence, it could be argued that the criteria specified for the use of normal concrete in the joints with headed bars could also be applied to the use of the self-consolidating concrete in these joints.
2. Irrespective of using normal concrete or self-consolidating concrete, the joints designed with the relative head area $\frac{A_{brg}}{A_b}$ of 3 (instead of 4) met the acceptance criteria of ACI 374-2005 [12] and ACI 318-14 [28] in terms of the seismic performance. The plastic hinge of the specimen with the self-consolidating concrete appeared farther away from the joint region, which suggested that it behaved better than the specimen with the normal concrete. In the specimen made with the self-consolidating concrete, this improvement was slightly more pronounced. Both of the specimens with the reduced relative head area had more than acceptable joint efficiency and the one with the self-consolidating concrete even had about 3% more efficiency than the control specimen. From these results, it could be concluded that for these joints, the relative head area of $\frac{A_{brg}}{A_b} = 3$ satisfied the seismic criteria regardless of whether the joint was made with the self-consolidating concrete or the normal one.
3. Self-consolidating concrete is not only easy to place, but also enhances the efficiency and the loading capacity of the joint. According to the results of this study, using the self-consolidating concrete instead of the normal one in the joints with headed bars improved their capacity by about 4%.
4. In both specimens made with the self-consolidating concrete, strength degradation started from the lower drifts, probably because of the properties of this concrete which made it susceptible to early cracking. But as loading was continued and higher drifts emerged, both of these specimens showed better ductility, efficiency, strength and generally, a better seismic behavior in comparison to those of the specimens made with the normal concrete.
5. Comparison of the M_{peak} extracted from the test results with the M_P of the joint specimens showed that they were all in compliance with the strong column-weak beam principle.
6. All specimens exhibited a ductile behavior, and none of them showed strength degradation in the drifts of less than 3.5%. All joint specimens in both normal concrete and self-consolidating concrete groups satisfied the acceptance criteria specified in ACI 374-2005 [12]; therefore, they can be considered suitable for use in the seismic areas.
7. Overall, for the joints with headed bars, it is possible to achieve a suitable seismic behavior with the reduced reinforcement congestion by (a) replacing the normal concrete with the self-consolidating one and (b) reducing the relative head area to about $\frac{A_{brg}}{A_b} = 3$.

Declaration of Competing Interest

None.

References

[1] Mahmoud Sayed. A Horizontally connected high-rise buildings under earthquake loadings. Ain Shams Eng J 2019;10(1):227–41.
[2] Parsa E, Sharbatdar MK, Kheyroddin A. Investigation of the flexural behavior of RC frames strengthened with HPFRCC subjected to lateral loads. Iran J Sci Technol Trans Civ Eng 2018. doi: https://doi.org/10.1007/s40996-018-0133-0.
[3] Maheri MR, Yazdani S. Seismic performance of different types of connections between steel bracing and RC frames. Iran J Sci Technol Trans Civ Eng 2016;40:287. doi: https://doi.org/10.1007/s40996-016-0034-z.
[4] Ghali A, Youakim SA. Headed studs in concrete: state of the art. ACI Struct J 2005;102(5):657–67.
[5] Wright JL, McCabe SL. The development length and anchorage behavior of headed reinforcing bars. In: University of Kansas Center for Research. Lawrence, Kansas; 1997. p. 154
[6] DeVries RA. Anchorage of headed reinforcement in concrete. University of Texas at Austin; 1996.
[7] Thompson MK, Jirsa JO, Breen JE. Behavior and capacity of headed reinforcement. ACI Struct J 2006;103(4):522–30.
[8] Thompson MK, et al. The anchorage behavior of headed reinforcement in CCT nodes and lap splices. Center for Transportation Research Report 1855-2. Austin, Texas; 2002.
[9] Kang THK, Sang SH, Choi DU. Bar pullout tests and seismic tests of small-headed bars in beam-column joints. ACI Struct J 2010;107(1):32–42.
[10] Wallace JW et al. Use of Headed reinforcement in beam-column joints subjected to earthquake loads. ACI Struct J 1998;95(5):590–606.
[11] Kang THK, Shin M, Kim W. Cyclic testing for seismic design guide of beam-column joints with closely spaced headed bars. J Earthquake Eng 2012;16 (2):211–30.
[12] ACI-Committee-374. Acceptance Criteria for Moment Frames Based on Structural Testing and Commentary. Farmington Hills, Michigan; 2005.
[13] Brooker O. Use of headed bars as anchorage to reinforcement. Struct Eng 2013:49–57.
[14] fib. fib model code for concrete structures 2010; 2013. p. 402.
[15] Chiu CK, Chi KN, Lin KC. Experimental investigation on the seismic anchorage behavior of headed bars based on full-size specimens of exterior and interior beam–column joints. Adv Struct Eng 2016;19(5):777–94.
[16] Lee HJ, Chen HC, Syu JH. Seismic performance of emulative precast concrete beam–column connections with alternative reinforcing details. Adv Struct Eng 2017;20(12):1793–806.
[17] Vella JP, Vollum RL, Kotecha R. Headed bar connections between precast concrete elements: design recommendations and practical applications. Structures 2018;15:162–73.
[18] Chun SC. Lap splice tests using high-strength headed bars of 550 MPa (80 ksi) yield strength. ACI Struct J 2015;112(5).
[19] Li L, Jiang Z. Flexural behavior and strut-and-tie model of joints with headed bar details connecting precast members. Perspect Sci 2016;7:253–60.
[20] Yang Y. Shear strength and behavior of reinforced concrete structures with T-headed bars in safety-related nuclear facilities [Doctoral Thesis]. West Lafayette, Indiana: Purdue University; 2015. p. 251.
[21] Lequesne R et al. Use of Headed Bars as Shear Reinforcement. Lawrence, KS: University of Kansas Center for Research, Inc; 2018.
[22] Mitchell D et al. Confinement of columns and wall boundary elements using headed bars. ASCE J Struct Eng 2014;140(3):1–9.
[23] Kim YH et al. Repeated loading tests of concrete walls containing headed shear reinforcement. ASCE J Struct Eng 2004;130(8):140.
[24] Mobin JS, Kazemi MT, Attari NKA. Cyclic behaviour of interior reinforced concrete beam-column connection with self-consolidating concrete. Struct Concr: J FIB 2016;17(4):618–29.
[25] Okamura H, Ouchi M. Self-consolidating concrete. J Adv Concr Technol 2003;1 (1):5–15.
[26] Dhakal RP, Ashtiani MS, Scott AN. Seismic performance of high-strength selfcompacting concrete in reinforced concrete beam-column joints, verification and utilization. In: 15th world conference on earthquake engineering 2012, 15WCEE. Lisbon, Portugal; 2012.
[27] Chien HL et al. Self-consolidating concrete columns under concentric compression. ACI Struct J 2008;105(4):425–32.
[28] ACI-Committee-318. Building Code Requirements for Structural Concrete (ACI 318–14) and Commentary (ACI 318R–14). Farmington Hills, Michigan, USA; 2014.
[29] ASTM International. A370-10 Standard Test Methods and Definitions for Mechanical Testing of Steel Products. ASTM International; 2006.

Abdolhossein Paknejadi is currently a Ph.D. candidate in the Pardis college, Civil Engineering Group at the Isfahan University of Technology, Isfahan, Iran. He received his BS and MS in civil engineering from the Islamic Azad University in Iran in 2004 and 2008. His research interests include seismic design of reinforced concrete structures.

Kiachehr Behfarnia, He is currently an Associate Professor at the Isfahan University of Technology, Isfahan, Iran and the head of department of civil engineering. He received his BS and MS in civil engineering from the Isfahan University of Technology, Isfahan, Iran in 1987, 1990, respectively and his Ph.D. in Structural Engineering from the University of NSW, Sydney, Australia in 1996. His research interests include analysis and design of reinforced and prestressed Concrete Structures and advanced concrete technology.